Editors' Suggestion | Featured in Physics

Entanglement-Enhanced Magnetic Induction Tomography

Wenqiang Zheng,[1,2] Hengyan Wang,[1,3] Rebecca Schmieg,[1] Alan Oesterle,[1] and Eugene S. Polzik[1,*]
[1]Niels Bohr Institute, University of Copenhagen, Blegdamsvej 17, 2100 Copenhagen ø, Denmark
[2]Zhejiang Provincial Key Laboratory and Collaborative Innovation Center for Quantum Precision Measurement, College of Science, Zhejiang University of Technology, Hangzhou 310023, China
[3]Department of Physics, Zhejiang University of Science and Technology, Hangzhou 310023, China

(Received 27 October 2022; accepted 4 April 2023; published 16 May 2023)

Magnetic induction tomography (MIT) is a sensing protocol exploring conductive objects via their response to radio-frequency magnetic fields. MIT is used in nondestructive testing ranging from geophysics to medical applications. Atomic magnetometers, employed as MIT sensors, allow for significant improvement of the MIT sensitivity and for exploring its quantum limits. Here, we propose and verify a quantum-enhanced version of the atomic MIT by combining it with conditional spin squeezing and stroboscopic backaction evasion. We use this quantum enhancement to demonstrate sensitivity beyond the standard quantum limits of one-dimensional quantum MIT detecting a conductive sample.

DOI: 10.1103/PhysRevLett.130.203602

Magnetic induction tomography (MIT) [1] uses a radio-frequency (rf) magnetic field from a coil to induce eddy currents in an object of interest. Detection of eddy currents allows one to reveal information about the composition and shape of an object nondestructively and noninvasively since the eddy currents depend on conductivity and permeability. While the bulk of MIT applications detects the eddy currents using a pickup coil, atomic rf magnetometers (AM) have been introduced as viable high-sensitivity alternative sensors for MIT [2–6].

Quantum sensing and metrology is one of the major fields within quantum information technologies [7]. It exploits quantum states of light and matter, such as entanglement and squeezing, to improve the sensitivity of sensors beyond the standard quantum limits (SQL), the boundaries existing in the absence of quantum correlations. Within atomic physics, quantum enhancement of sensitivity has been demonstrated for interferometry [8,9], electric field sensing [10], clocks [11–13], and magnetometers [14–16].

Here, we demonstrate a novel application of quantum metrology, quantum-enhanced magnetic induction tomography (QMIT). The protocol exploits (1) implementing an anti-Helmholtz coil geometry providing efficient cancellation of classical noise [6], (2) introducing a stroboscopic measurement sequence at an rf rate suppressing quantum backaction, (3) generation of spin-squeezed states of the atomic spin sensor, and (4) measuring the eddy current signal compatible with the stroboscopic measurement sequence.

For a sensor containing N_A uncorrelated particles, such as atomic spins, the SQL of measurement sensitivity scales as $1/\sqrt{N_A}$ [17]. It is set by the Heisenberg uncertainty principle restricting how precisely two noncommuting operators can be measured simultaneously. Spin squeezing and entanglement can improve the sensitivity beyond the $1/\sqrt{N_A}$ limit. While large spin ensembles with $\sqrt{N_A} \gg 1$ promise the most sensitive measurements, technical imperfections growing with N_A often preclude overcoming the SQL. Reduced technical fluctuations make the SQL more attainable for measurements in the rf range [18]. As MIT uses rf field sensing, quantum enhancement appears to be an attractive approach for enhancing the sensitivity.

The experimental setup of QMIT is shown in Fig. 1. The atomic sensor, containing N_A cesium atoms inside a vapor cell, is placed inside a bias magnetic field B_{bias} along the x axis corresponding to $\Omega_L \approx 2\pi \cdot 725$ kHz Larmor frequency. The protocol is facilitated by the long transverse spin relaxation time $T_2 \approx 2.35$ ms, which is due to the anti-relaxation-coated cell walls [19]. Optical pumping prepares the ensemble in a coherent spin state (CSS) with $m_F = F = 4$, for which $J_x = \langle \hat{J}_x \rangle = \sum_{k=1}^{N_A} \langle \hat{j}_x^k \rangle = FN_A$, where $\hat{j}_x^k$ refers to the kth atom's spin. The AM is placed in between two anti-Helmholtz rf coils and monitors the magnetic field response $\vec{B}_{\mathrm{ec}}$ generated by the eddy currents induced in the conductive object [Fig. 1(a)]. In the absence of an object, the total rf field is zero at the location of the sensor and hence no transverse spin component is driven. The minimal quantum fluctuation for uncorrelated spins, corresponding to the projection noise (PN) $\mathrm{Var}(\hat{J}_y) = \mathrm{Var}(\hat{J}_z) = (F/2)N_A$ arising from the Heisenberg uncertainty principle, limits the sensitivity of the AM.

In the presence of a conductive object, a nonzero transverse spin component $\vec{J}_\perp$ is created [Fig. 1(c)]:

$$\langle \vec{J}_\perp \rangle = \frac{\gamma}{2} B_{\mathrm{ec}} J_x T_2 [1 - \exp(-\tau/T_2)], \tag{1}$$

where τ is the duration of the rf pulse, T_2 is the transverse spin coherence time, and γ is the gyromagnetic ratio.

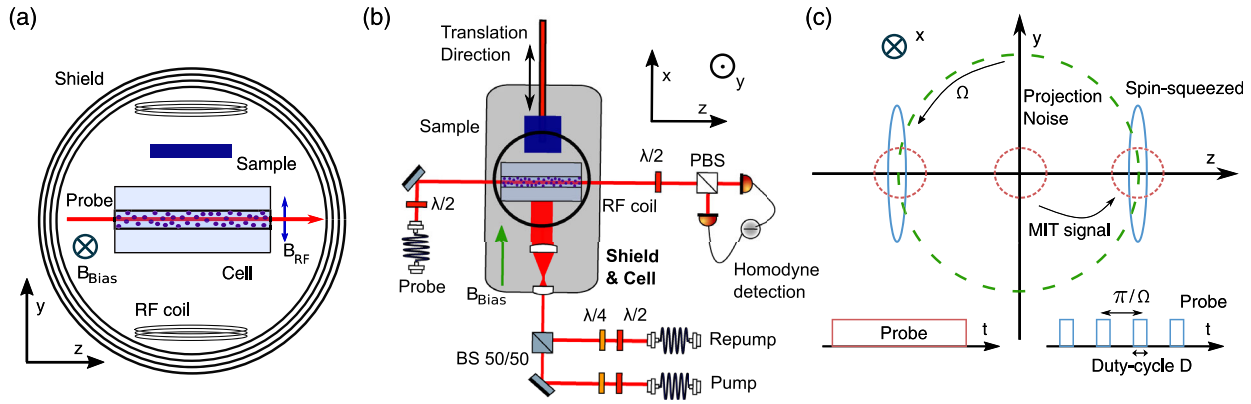

FIG. 1. Setup for entanglement-enhanced MIT. (a) Configuration of rf coils, the probing direction, the bias magnetic field, the conductive sample, and the vapor cell inside the magnetic shield. (b) Simplified experimental setup (top view), where $\lambda/2$ and $\lambda/4$ indicate half- and quarter-wave plates, (P)BS indicates a (polarizing) beam splitter. (c) Illustration of the trajectory of the spin projection $\vec{J}_\perp$ (dashed green line) in the presence of the MIT signal, together with the PN of the CSS state (red) and the squeezed state (blue). The insets show the time sequences for the continuous and stroboscopic probing. More visualizations of spin dynamics and quantum noise can be found in Supplemental Material [20].

Monitoring $\vec{J}_\perp$ by polarization homodyne detection [Fig. 1(b)] allows extracting information about the induced eddy currents, and hence about the properties of the sample. With the probe light far detuned from any atomic transition, we can realize a quantum nondemolition (QND) measurement of the spin component $\vec{J}_z$ via Faraday interaction $\hat{H}_F \propto (\kappa/\sqrt{N_A N_P})\hat{S}_z\hat{J}_z$ [24], where $\kappa \propto \sqrt{N_A N_P}$ is the coupling constant and $N_P(N_A)$ is the photon (atom) number. $\hat{S}_z$ is the Stokes operator of the probe light whose value is equal to the difference between right- and left-hand circular polarized components. The Stokes operators obey $[\hat{S}_z, \hat{S}_y] = iS_x$, where S_x can be treated as a number for input light polarized along x axis.

The homodyne detection yields the Stokes operator $\hat{S}_y^{\text{out}} \propto \hat{J}_z = \hat{J}_{z_0}\cos(\Omega t) + \hat{J}_{y_0}\sin(\Omega t)$. Here, $\hat{J}_{z_0}$ and $\hat{J}_{y_0}$ are the spin projections in the rotating frame satisfying $[\hat{J}_{z_0}, \hat{J}_{y_0}] = iJ_{x0} = iFN_A$. For continuous probing, $\hat{J}_{z_0}$ and $\hat{J}_{y_0}$ are measured with alternating strength proportional to $\sin(\Omega t)$ and $\cos(\Omega t)$ per Larmor precession, respectively. Simultaneously, extraneous quantum backaction noise (BAN) is imprinted onto the conjugate components $\hat{J}_{z_0}$ and $\hat{J}_{y_0}$ via light-atom interaction [25]. In the laboratory frame, as $\vec{J}_\perp$ rotates around $\vec{B}_{\text{bias}}$ at the frequency Ω, BAN is imprinted onto both spin components $\vec{J}_y$ and $\vec{J}_z$, and thus affects the readout noise of the polarization homodyning. Quantum fluctuations of light, corresponding to the photon shot noise (SN), increase the measurement uncertainty also. Therefore, continuous measurement of a precessing spin suffers from SN, PN, and BAN [26]. The total quantum noise of the cosine quadrature of the Stokes component ($\hat{S}_y^{\text{out}}$), recorded by a lock-in amplifier (LIA), can be expressed as

$$\text{Var}(\hat{S}_{y,c}^{\text{out}}) \approx \frac{N_P}{4}\left(1 + \frac{\kappa^2}{2} + \frac{\kappa^4}{12}\right), \tag{2}$$

where the three terms correspond to SN, PN, and BAN, respectively. As the signal grows linearly with κ, the SQL of a continuous measurement is achieved for $\kappa^4 = 12$, which optimizes the signal-to-noise ratio $\text{SNR} \propto \kappa/\sqrt{1 + \kappa^2/2 + \kappa^4/12}$. The respective SQL of the total noise variance is thus $2(1 + \kappa^2/2 + \kappa^4/12)/\kappa^2 = 1 + 2/\sqrt{3}$ times greater than the projection noise variance and the standard deviation is approximately 1.47 times greater.

A time-dependent measurement, e.g., a stroboscopic measurement, enables backaction free measurement of one spin component with a sensitivity exceeding the SQL [25,27,28]. For stroboscopic probing at twice the Larmor frequency [25], illustrated in Fig. 1(c), quantum noise of the probe observable takes the following form:

$$\text{Var}(\hat{S}_{y,c}^{\text{out}}) \approx \frac{\eta N_P}{4}\left(1 + \frac{\tilde{\kappa}^2}{2} + C\frac{\tilde{\kappa}^4}{12}\right), \tag{3}$$

where $\eta = 1 + \text{sinc}(\pi D)$, D is the duty cycle of stroboscopic probing, $\tilde{\kappa} = \sqrt{\eta}\kappa$, and $C = \{[1 - \text{sinc}(\pi D)]/[1 + \text{sinc}(\pi D)]\}$. For a δ pulse ($D = 0$), perfect quantum backaction evasion is achieved, allowing for a QND measurement to be realized. The magnetic sensitivity for the eddy current detection then approaches $\delta B_{\text{ec}} \propto 1/\text{SNR} \propto \sqrt{(1 + \tilde{\kappa}^2/2)}/\tilde{\kappa}$.

As a first step, we verify a spin-squeezed state of the atoms contained in an interaction volume of 500 μm × 500 μm × 25 mm using the sequence shown in Fig. 2(a). The ensemble consists of 1.5×10^9 atoms at the temperature of 55 °C. Using optical pumping [20], the atoms are

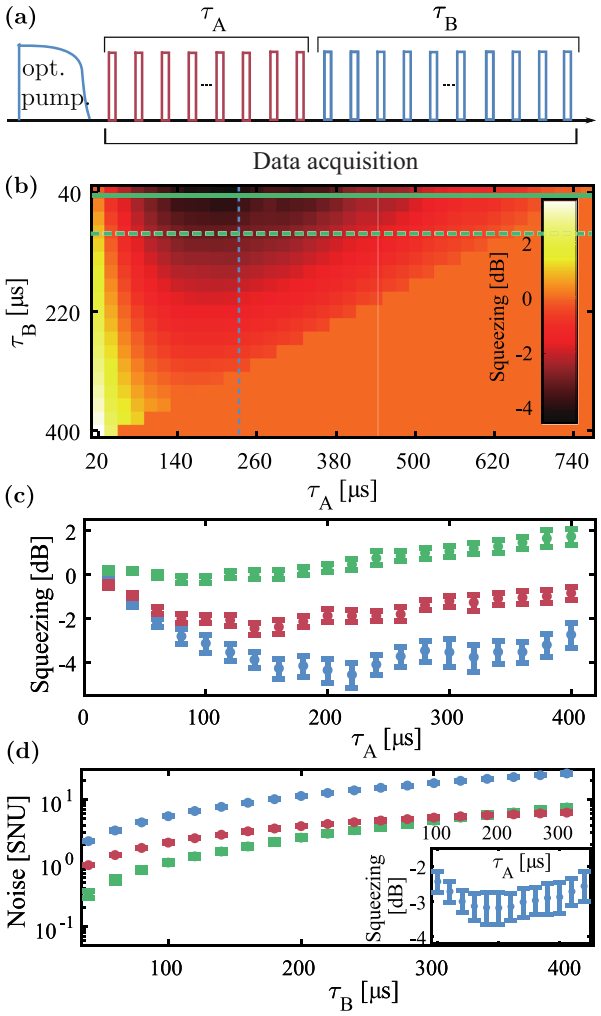

FIG. 2. Generation of a spin-squeezed state of the magnetometer. (a) Pulse sequence used for squeezing demonstration consisting of optical pumping and a train of stroboscopic probing pulses modulated at twice the Larmor frequency. (b) Experimental demonstration of squeezing versus preparation duration τ_A and verification duration τ_B for 15% duty cycle. Green horizontal line (solid): slice for $\tau_B = 40$ μs used in subfigure (c). Blue vertical line: slice for $\tau_A = 220$ μs used in subfigure (d). Green horizontal line (dashed): slice used for inset in subfigure (d). (c) Achievable squeezing versus τ_A for $\tau_B = 40$ μs for 15% (blue), 50% (red), and 90% (green) duty cycle. (d) Projection noise (red), unconditional variance (blue), and conditional variance (green) versus τ_B for optimal $\tau_A = 220$ μs. The noise is normalized to light shot noise units (SNU). The inset shows squeezing for $\tau_B = 100$ μs versus τ_A. The error bars in subfigures (c) and (d) are obtained from statistical analysis of eight datasets, each containing 4000 repetitions.

prepared in the CSS. Typically, we achieve an atomic polarization of 97.5%, verified by pulsed magneto-optical resonance spectroscopy [20]. The imperfection leads to the spin projection noise 19.5% higher than that of the CSS [20]. The spin noise is calibrated using the measured spin noise of the unpolarized atomic ensemble, namely the thermal spin state, since the thermal spin state is insensitive to classical noise and BAN [20].

Optical pumping is followed by two sequences of stroboscopic probing pulses, modulated at $2\Omega_L$ with varying duty cycles, generated using acousto-optical modulators. The probe laser is locked with a detuning of 1.95 GHz from the $F = 4 \rightarrow F' = 4, 5$ crossover transition of the D2 line. The first stroboscopic sequence with duration τ_A prepares a squeezed state via QND measurement, while the second sequence with duration τ_B verifies the degree of spin squeezing when conditioning on the outcome of the first stroboscopic measurement. The sequence is repeated thousands of times, allowing us to estimate $\langle \vec{J}_\perp \rangle$. The signal of each individual sequence is demodulated using a LIA and then recorded. Here, the outcomes are denoted Q_A and Q_B for the squeezing generation and verification processes, respectively. Conditioning the signal Q_B during τ_B on the preceding signal Q_A during τ_A, allows one to determine the conditional variance

$$\begin{aligned} \mathrm{Var}(Q_B|Q_A) &= \min[\mathrm{Var}(Q_B - \alpha Q_A)] \\ &= \mathrm{Var}(Q_B - \alpha_{\mathrm{opm}} Q_A) \\ &= \mathrm{Var}(Q_B) - \frac{\mathrm{Cov}^2(Q_B, Q_A)}{\mathrm{Var}(Q_A)}, \end{aligned} \tag{4}$$

where α is the feedback parameter whose optimal value $\alpha_{\mathrm{opm}} = [\mathrm{Cov}(Q_B, Q_A)/\mathrm{Var}(Q_A)]$ minimizes the conditional variance.

From the conditional and unconditional variances during τ_B, we find the degree of spin squeezing as

$$\xi^2 = \frac{\mathrm{Var}(Q_B|Q_A) - \mathrm{SN}_B - \mathrm{EN}_B}{\mathrm{Var}(Q_B) - \mathrm{SN}_B - \mathrm{EN}_B}, \tag{5}$$

where SN_B and EN_B are photon shot noise and electronic noise contributions during the verifying process. With the reduced conditional variance, the quantum noise limited sensitivity increases to $\delta B_{\mathrm{ec}} \propto \sqrt{(1 + \xi^2 \tilde{\kappa}^2/2)}/\tilde{\kappa}$.

The degree of spin squeezing is optimized by varying τ_A and τ_B as shown in Fig. 2(b). There is a clear optimum for the squeezing preparation time τ_A due to two opposing effects. For a too short τ_A, the measurement strength limits the obtained information about the atomic spin and thus the degree of squeezing. Extending τ_A too long leads to additional decoherence and depumping effects. The increase of τ_B beyond an optimal value degrades the level of squeezing due to the information loss by decoherence effects. For the optimal values $\tau_A = 220$ μs and $\tau_B = 40$ μs, we observe $10\log(\xi^2) = (-4.6 \pm 0.6)$ dB of spin squeezing. Plotting the level of squeezing for $\tau_B = 40$ μs versus the duration of τ_A for different duty cycles D of the stroboscopic pulses, we observe squeezing degradation due to worse backaction evasion [Fig. 2(c)].

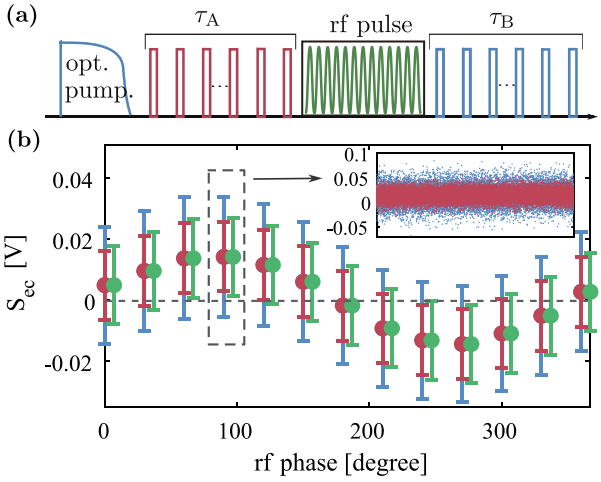

FIG. 3. Entanglement-enhanced eddy current measurement. (a) Pulse sequence with rf pulse between stroboscopic probing pulses. (b) Eddy current signals (S_{ec}), the difference between sample and background signals, as a function of the rf phase. Each point is averaged over 16 000 measurements, while error bars represent single-shot uncertainty. Blue and red points represent unconditional and conditional results, respectively. The green error bars represent the quantum noise $\sqrt{SN_B + PN_B}$, corresponding to the backaction evaded measurement without squeezing, horizontally shifted for clarity. The inset shows the unconditional (blue) and conditional (red) signal distribution for the rf phase of 90°.

The degree of spin squeezing together with the atomic polarization allows us to estimate the degree of entanglement present in the macroscopic spin ensemble [29]. With squeezing of (-4.6 ± 0.6) dB and an initial atomic polarization of > 0.97, we find that the spin ensemble contains groups of up to ten entangled atoms. The non-negligible level of SN weakens the effect of the spin squeezing on the overall observed noise. For $\tau_B = 40$ μs in Fig. 2(d), SN and PN are of similar magnitude. Increasing τ_B to 100 μs improves the overall noise reduction in the conditional variance, enabling a more efficient measurement of a conductive sample at the expense of spin squeezing.

Next, we exploit spin squeezing to demonstrate QMIT with sensitivity improved beyond the projection noise limit. For this, an rf pulse of 47 μs duration, with a frequency matching the Larmor frequency ν_L is introduced in between the two stroboscopic measurements [Fig. 3(a)]. For optimal measurement efficiency, the stroboscopic pulses are required to overlap with the cosine quadrature of the LIA reference signal. Further, the eddy current detection is optimal when the rf pulse phase matches the LIA reference signal [Fig. 3(b)].

The rf field induces eddy currents in the sample, a small titanium piece of dimension 1 mm × 10 mm × 10 mm. Figure 3(b) visualizes the MIT signal from the sample as a function of the phase of the rf field. The signal is the difference between the sample and background measurement. The eddy current signal is maximal with an out-of-phase rf field. The respective uncertainties for conditional (red) and unconditional (blue) measurements are shown in Fig. 3(b). For comparison, the quantum noise for the backaction evaded measurement without squeezing is shown in green. It is determined from the experimental results as $\sqrt{SN_B + PN_B}$, where PN_B is the projection noise variance during τ_B and SN_B is the shot noise variance as defined in Eq. (5). The average level of spin squeezing for the data shown in Fig. 3(b) is (-1.8 ± 0.1) dB. The observed reduction in the level of squeezing originates from multiple factors. First, introducing a gap leads to a degradation of squeezing due to decoherence effects [20]. For a gap of 50 μs, squeezing is reduced to (-3.0 ± 0.4) dB when the rf coils are disconnected from electronic devices. The second effect reducing the available squeezing is the connection of the rf coils to the function generator. While connecting the coils compromises the squeezing, we did not observe a significant change between sending the rf pulse or not. We therefore believe the degradation of squeezing originates from minuscule currents flowing through the coils even when no rf pulse is sent from the function generator. Despite this, we still observe $(41 \pm 1)\%$ reduction between conditional to unconditional uncertainty. Considering the maximal signal at 90° rf phase, we observe 42.5% noise reduction, improving the SNR of a single-shot measurement from 0.72 to 1.2. The entanglement-assisted sensing allows us to achieve a conditional uncertainty 11% below the expected quantum noise for the backaction free measurement, given as $\sqrt{SN_B + PN_B}$. This result matches well with the sensitivity improvement expected from the level of squeezing, estimated through $\sqrt{SN_B + \xi^2 PN_B}/\sqrt{SN_B + PN_B} \approx 0.89$ [20]. Comparing the SQL of continuous measurements, given by $(1 + 2/\sqrt{3})^{1/2} \approx 1.47$ in

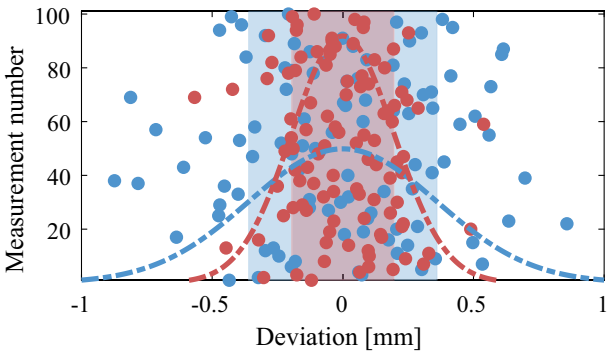

FIG. 4. Entanglement-enhanced 1D MIT. The statistical distribution of the sample center found from 1D MIT scanning 50 mm in 1 mm steps. One hundred red (blue) points corresponding to the results for the position of the center of the sample obtained with (without) spin entanglement. Each point is averaged over 40 measurement repetitions. The red (blue) shaded areas cover the red (blue) data points within one standard deviation.

units of $\sqrt{\mathrm{PN}_B}$ to our conditional noise of $1.11\sqrt{\mathrm{PN}_B}$, the observed noise reduction can be estimated as $1.11/1.47 = 0.76$, corresponding to -2.4 dB noise reduction.

Finally, we demonstrate the spatial sensitivity of our sensor with a one-dimensional (1D) QMIT of the sample. As shown in Fig. 1(b), the sample is moved past the cell in 1 mm steps along the x axis. For each position, 4000 consecutive measurements are performed. The conditional variance is determined using $\alpha_{\mathrm{opm}} = 0.91$ from the no-sample measurement. We average the sweep of the sample 40 times, corresponding to 100 independent MIT measurements. In Fig. 4, the distribution of the sample center for the 100 MIT measurements is shown with conditional and unconditional results marked in red and blue, respectively. The distribution is significantly narrower using spin squeezing, visualized using Gaussian distributions and shaded areas, reflecting the standard deviation of 0.20 mm for the conditional measurement and 0.36 mm for the unconditional measurement. The quantum-enhanced MIT provides a nearly twofold improvement in precision.

The duration of a single 1D tomography sequence can be estimated from the number of repetitions combined with the number of positions measured. Using a conservative estimate of 13 ms per repetition including optical pumping and the measurement, 40 repetitions per position would take 520 ms. The total scan sufficient to measure the sample position with an uncertainty of 0.20 mm would take 26 s.

We have proposed a novel quantum sensing protocol for magnetic induction tomography. We successfully demonstrated entanglement-enhanced eddy current detection and 1D QMIT through backaction evasion and spin squeezing. The demonstrated improvement of sensitivity beyond the SQL offers a promising path toward noninvasive measurements on weakly conducting samples, such as biological tissue, exploiting the noise reduction for higher sensitivity and less measurement time.

The authors would like to thank Kasper Jensen for valuable input and discussion on both experimental implementation and theoretical understanding. The authors acknowledge many fruitful discussions with Jörg Helge Müller and Jean-Baptiste Beguin. Mikhail Balabas fabricated the alkene coated vapor cell used for this experiment. We acknowledge funding by the Novo Nordisk Foundation grant NNF20OC0064182 within the "Exploratory Interdisciplinary Synergy Programme 2020," the EU grant MacQsimal, the European Research Council (ERC) under the EU Horizon 2020 programme (Grant no. 787520), and the VILLUM FONDEN under a Villum Investigator Grant (Grant no. 25880). W. Z. and H. W. acknowledge the support of the National Nature Science Foundation of China (Grant no. 12075206).

W. Z., H. W., and R. S. contributed equally to this work.

*Corresponding author.
polzik@nbi.ku.dk

[1] H. Griffiths, Magnetic induction tomography, Meas. Sci. Technol. **12**, 1126 (2001).
[2] A. Wickenbrock, S. Jurgilas, A. Dow, L. Marmugi, and F. Renzoni, Magnetic induction tomography using an all-optical 87 rb atomic magnetometer, Opt. Lett. **39**, 6367 (2014).
[3] C. Deans, L. Marmugi, S. Hussain, and F. Renzoni, Electromagnetic induction imaging with a radio-frequency atomic magnetometer, Appl. Phys. Lett. **108**, 103503 (2016).
[4] A. Wickenbrock, N. Leefer, J. W. Blanchard, and D. Budker, Eddy current imaging with an atomic radio-frequency magnetometer, Appl. Phys. Lett. **108**, 183507 (2016).
[5] C. Deans, L. Marmugi, and F. Renzoni, Through-barrier electromagnetic imaging with an atomic magnetometer, Opt. Exp. **25**, 17911 (2017).
[6] K. Jensen, M. Zugenmaier, J. Arnbak, H. Stærkind, M. V. Balabas, and E. S. Polzik, Detection of low-conductivity objects using eddy current measurements with an optical magnetometer, Phys. Rev. Res. **1**, 033087 (2019).
[7] C. Degen, F. Reinhard, and P. Cappellaro, Quantum sensing, Rev. Mod. Phys. **89**, 035002 (2017).
[8] J. Estève, C. Gross, A. Weller, S. Giovanazzi, and M. K. Oberthaler, Squeezing and entanglement in a Bose–Einstein condensate, Nature (London) **455**, 1216 (2008).
[9] J. Appel, P. J. Windpassinger, D. Oblak, U. B. Hoff, N. Kjærgaard, and E. S. Polzik, Mesoscopic atomic entanglement for precision measurements beyond the standard quantum limit, Proc. Natl. Acad. Sci. U.S.A. **106**, 10960 (2009).
[10] K. A. Gilmore, M. Affolter, R. J. Lewis-Swan, D. Barberena, E. Jordan, A. M. Rey, and J. J. Bollinger, Quantum-enhanced sensing of displacements and electric fields with two-dimensional trapped-ion crystals, Science **373**, 673 (2021).
[11] A. Louchet-Chauvet, J. Appel, J. J. Renema, D. Oblak, N. Kjaergaard, and E. S. Polzik, Entanglement-assisted atomic clock beyond the projection noise limit, New J. Phys. **12**, 065032 (2010).
[12] A. Derevianko and H. Katori, Colloquium: Physics of optical lattice clocks, Rev. Mod. Phys. **83**, 331 (2011).
[13] M. Schioppo *et al.*, Ultrastable optical clock with two cold-atom ensembles, Nat. Photonics **11**, 48 (2017).
[14] H. Bao *et al.*, Spin squeezing of 1011 atoms by prediction and retrodiction measurements, Nature (London) **581**, 159 (2020).
[15] W. Wasilewski, K. Jensen, H. Krauter, J. J. Renema, M. V. Balabas, and E. S. Polzik, Quantum Noise Limited and Entanglement-Assisted Magnetometry, Phys. Rev. Lett. **104**, 133601 (2010).
[16] R. J. Sewell, M. Koschorreck, M. Napolitano, B. Dubost, N. Behbood, and M. W. Mitchell, Magnetic Sensitivity Beyond the Projection Noise Limit by Spin Squeezing, Phys. Rev. Lett. **109**, 253605 (2012).
[17] D. Budker and M. Romalis, Optical magnetometry, Nat. Phys. **3**, 227 (2007).
[18] I. Savukov, S. Seltzer, and M. Romalis, Detection of nmr signals with a radio-frequency atomic magnetometer, J. Magn. Reson. **185**, 214 (2007).

[19] M. Balabas, K. Jensen, W. Wasilewski, H. Krauter, L. S. Madsen, J. H. Müller, T. Fernholz, and E. S. Polzik, High quality anti-relaxation coating material for alkali atom vapor cells, Opt. Express **18**, 5825 (2010).

[20] See Supplemental Material at http://link.aps.org/supplemental/10.1103/PhysRevLett.130.203602 for details of the experimental setup, calibration of the spin noise, verification of the back action evasion, and data on the spin state decay, which includes Refs. [21–23].

[21] B. Julsgaard, J. Sherson, J. L. Sørensen, and E. S. Polzik, Characterizing the spin state of an atomic ensemble using the magneto-optical resonance method, J. Opt. B **6**, 5 (2003).

[22] B. Julsgaard, Entanglement and quantum interactions with macroscopic gas samples, Ph.D. thesis, University of Aarhus, 2003.

[23] D. A. Steck, Cesium D Line Data, http://steck.us/alkalidata (revision 2.2.1, November 2019).

[24] K. Hammerer, A. S. Sørensen, and E. S. Polzik, Quantum interface between light and atomic ensembles, Rev. Mod. Phys. **82**, 1041 (2010).

[25] G. Vasilakis, H. Shen, K. Jensen, M. Balabas, D. Salart, B. Chen, and E. S. Polzik, Generation of a squeezed state of an oscillator by stroboscopic back-action-evading measurement, Nat. Phys. **11**, 389 (2015).

[26] K. Hammerer, E. Polzik, and J. I. Cirac, Teleportation and spin squeezing utilizing multimode entanglement of light with atoms, Phys. Rev. A **72**, 052313 (2005).

[27] V. B. Braginsky, Y. I. Vorontsov, and K. S. Thorne, Quantum nondemolition measurements, Science **209**, 547 (1980).

[28] C. Meng, G. A. Brawley, J. S. Bennett, M. R. Vanner, and W. P. Bowen, Mechanical Squeezing via Fast Continuous Measurement, Phys. Rev. Lett. **125**, 043604 (2020).

[29] A. S. Sørensen and K. Mølmer, Entanglement and Extreme Spin Squeezing, Phys. Rev. Lett. **86**, 4431 (2001).